Globally Optimal Linear Approach to the Design of Heat Exchangers Using Threshold Fouling Modeling

Julia C. Lemos and André L. H. Costa
Institute of Chemistry, Rio de Janeiro State University (UERJ) Rua São Francisco Xavier, 524, Maracanã, Rio de Janeiro. RJ CEP 20550-900, Brazil

Miguel J. Bagajewicz
School of Chemical, Biological and Materials Engineering, University of Oklahoma, Norman, OK 73019

DOI 10.1002/aic.16083
Published online in Wiley Online Library (wileyonlinelibrary.com)

This article presents a method for the mathematical optimization of the design of heat exchangers including fouling rate modeling for the tube-side. The description of the fouling rate in crude preheat trains of petroleum distillation units is commonly based on threshold models (Ebert-Panchal model and its variants). Our formulation of the design problem employs a mixed-integer linear programing approach; therefore the solution is the global optimum and common non-convergence drawbacks of mixed-integer nonlinear programming models are totally avoided. Three different examples are employed to compare the proposed approach with an optimization procedure using fixed fouling resistances. The results indicate that in two problems was possible to obtain design solutions associated to smaller heat exchangers. Additionally, three case studies are also explored to discuss how fouling is related to crude types, pressure drop manipulation, and energy integration. © 2018 American Institute of Chemical Engineers *AIChE J*, 00: 000–000, 2018
Keywords: optimization, design, heat transfer

Introduction

The traditional approach for the design of shell-and-tube heat exchangers involves a trial-and-error procedure, where successive candidate solutions are generated until a feasible option is found that fulfills thermal and hydraulic specifications.[1–3] However, the utilization of optimization techniques can bring important cost reductions in the design of shell-and-tube heat exchangers.[4] Therefore, the development of automatic procedures for the design of heat exchangers using optimization algorithms was the subject of many articles. For example, focusing only on mathematical programming solutions, there are nonlinear programming (NLP) methods,[5,6] mixed-integer nonlinear programming (MINLP) methods,[7–9] mixed-integer linear programming (MILP),[10] and integer linear programming (ILP) methods.[11]

An important issue in the heat exchanger design problem is the need to accommodate the impact of fouling in the solution. Despite the complexity of the fouling behavior, almost all previous design procedures handle this aspect of the problem using fixed suggested values of fouling resistances, for example, TEMA values.[12] However, the utilization of conventional fixed fouling resistances are subjected to considerable criticism, as pointed out by Shilling.[13]

A more recent approach to handle the impact of fouling in the design is to include fouling modeling directly and simultaneously in the design procedure. This approach explores the variation of the fouling resistance with the thermofluid dynamic conditions of the heat exchanger, that is, different heat exchanger candidates for the same thermal service may present different fouling resistances.

Among all the efforts, the interconnection between fouling modeling and heat exchanger design procedures was particularly explored in the analysis of the design of shell-and-tube heat exchangers in crude preheat trains using a threshold model.[14–17] Crude preheat trains are heat exchanger networks employed to reduce the energy consumption of the fired heater in petroleum distillation units. The accumulation of deposits in these equipment reduces the coil inlet temperature, bringing an increase of fuel costs.

Butterworth[14] used a graphical method to design heat exchangers considering the influence of temperature and velocity in the fouling rate, according to the threshold behavior. Three different cases for the design were explored: a "no fouling" design, an asymptotic fouling behavior, and a fouling resistance defined according to a constant wall temperature and flow velocity during the operational campaign. The insertion of a threshold model in the analysis of the heat exchanger design using a graphical tool was also investigated by Polley et al.[15]

Polley et al.[16] pointed out the importance to design heat exchangers in crude preheat trains able to achieve process specifications during the entire campaign, thus avoiding costly throughput losses. They proposed a procedure where, initially,

Additional Supporting Information may be found in the online version of this article.

Correspondence concerning this article should be addressed to A. L. H. Costa at andrehc@uerj.br.

a heat exchanger design in a clean condition is obtained using a graphical tool and, then, an extension of this heat exchanger is applied to a standard length with a higher area. The resultant design is then checked using a fouling rate model to identify if it fulfills satisfactorily the thermal task along the entire operational period.

Nakao et al.[17] proposed an iterative procedure using a commercial heat exchanger design software. After each solution provided by the software, a pseudostationary simulation of the heat exchanger was conducted to determine the value of the fouling resistance at the end of the campaign according to a threshold model. Then, the calculated value of the fouling resistance is employed in a new software run. The procedure is repeated until convergence is reached.

The different approaches in the literature presented above to include the fouling behavior do not guarantee optimality conditions. In terms of mathematical programming, the inclusion of fouling modeling in the optimization of the heat exchanger design was explored before by Lemos et al.[18] The fouling resistance model employed was a power law in relation to the velocity, adequate, for example, to describe the fouling resistance behavior in cooling water streams.[19] However, this model is not fully adequate to describe the fouling behavior in crude oil streams. The utilization of threshold models, where the influence of velocity and temperature can be considered, is much more complex, as it will be developed along the current article.

Aiming at filling this gap, we propose here an approach to design heat exchangers considering a threshold fouling model using mathematical programming. The approach is based on the extension of the ILP model proposed by Gonçalves et al.[11] Therefore, the design procedure can identify better solutions in crude preheat trains which may be associated to lower fouling resistances. The linear form of the optimization problem proposed is rigorously equivalent to the original nonlinear equations, which allows the identification of the global optimum of the corresponding design problem.

This article is organized as follows. We start presenting the heat exchanger and the threshold fouling models for the tube-side. Then, we discuss how a threshold fouling model can be accommodate in a linear form in the optimization problem. Therefore, the resultant MILP problem is then proposed and the corresponding numerical performance is illustrated by three examples and three case studies. At the end, we present the conclusions.

Heat Exchanger Model

This section shows the original heat exchanger equations employed in the optimization. The model is based on the following premises: one phase turbulent flow on the tube-side and the shell-side, single E-type shell associated to a number of tube passes equal to one or an even number, and constant physical properties. It is also assumed that the cold stream flows in the tube-side, according to the available threshold models, and the total fouling resistance is dominated by the cold stream fouling resistance (i.e., the hot stream fouling resistance is negligible).

The heat-transfer rate equation is based on the LMTD method.[20] The shell-side heat-transfer coefficient and pressure drop are calculated using the Kern model.[1] The tube-side heat transfer coefficient and the pressure drop are calculated using the Dittus-Boelter correlation[20] and the Darcy-Weisbach equation,[21] respectively. We used this set of thermofluid dynamic equations before.[10,11] The model constraints can be divided in six blocks: shell-side equations, tube-side equations, overall heat-transfer coefficient, heat-transfer rate equation, variable bounds, and geometric constraints. In the model presentation below, the corresponding parameters are represented using the symbol "^" on top.

Shell-side thermal and hydraulic constraints

The flow area between adjacent baffles (Ar) is described by the following constraint

$$Ar = Ds \ \mathrm{FAR} \ lbc \tag{1}$$

where Ds is the shell diameter, FAR is the free area ratio, and lbc is the baffle spacing. The expression for the FAR evaluation is

$$\mathrm{FAR} = \frac{(ltp - dte)}{ltp} = 1 - \frac{dte}{ltp} = 1 - \frac{1}{rp} \tag{2}$$

where ltp is the tube pitch, dte is the outer tube diameter, and rp is the pitch ratio.

The constraint concerning the shell-side velocity (vs) is

$$vs = \frac{\widehat{ms}}{\widehat{\rho s} \ Ar} \tag{3}$$

where $\widehat{ms}$ and $\widehat{\rho s}$ are the mass flow rate and the density of the fluid on the shell-side, respectively.

To calculate the Reynolds number, we first introduce the equivalent diameter (Deq) constraint, which depends on the tube pattern

$$Deq = \frac{4 \ ltp^2}{\pi \ dte} - dte \ (\mathrm{Square \ pattern}) \tag{4}$$

$$Deq = \frac{3.46 \ ltp^2}{\pi \ dte} - dte \ (\mathrm{Triangular \ pattern}) \tag{5}$$

Then, the Reynolds number for the shell-side (Res) is given by

$$Res = \frac{Deq \ vs \ \widehat{\rho s}}{\widehat{\mu s}} \tag{6}$$

where $\widehat{\mu s}$ is the viscosity of the fluid on the shell-side.

The convective heat-transfer coefficient depends on the Nusselt number (Nus), which is described by

$$Nus = 0.36 \ Res^{0.55} \widehat{Prs}^{1/3} \tag{7}$$

where $\widehat{Prs}$ is the Prandtl number of the shell-side stream.

Finally, the convective heat-transfer coefficient for the shell-side (hs) can be determined by

$$Nus = \frac{hs \ Deq}{\widehat{ks}} \tag{8}$$

The pressure drop in the shell-side (ΔPs) can be determined by

$$\frac{\Delta Ps}{\widehat{\rho s} \ \widehat{g}} = fs \frac{Ds(Nb + 1)}{Deq} \left(\frac{vs^2}{2 \ \widehat{g}} \right) \tag{9}$$

where $\widehat{g}$ is the gravity acceleration, fs is the friction factor, and Nb is the number of baffles. The friction factor and the number of baffles can be calculated by

$$fs = 1.728 \ Res^{-0.188} \tag{10}$$

$$Nb = \frac{L}{lbc} - 1 \tag{11}$$

where L is the tube length.

Tube-side thermal and hydraulic constraints

The velocity in the tube-side (vt) is

$$vt = \frac{4\ \widehat{mt}}{Ntp\ \pi\ \widehat{\rho t}\ dti^2} \tag{12}$$

where $\widehat{mt}$ and $\widehat{\rho t}$ are the mass flow rate and the density of the stream in the tube-side, Ntp is the number of tubes per pass, and dti is the inner diameter of the tubes.

The Reynolds number on the tube-side (Ret) is given by

$$Ret = \frac{dti\ vt\ \widehat{\rho t}}{\widehat{\mu t}} \tag{13}$$

where $\widehat{\mu t}$ is the viscosity of the stream in the tube-side.

The tube-side Nusselt number (Nut) is given by

$$Nut = 0.023\ Ret^{0.8}\widehat{Prt}^{n} \tag{14}$$

where the parameter n is equal to 0.3 for cooling services and 0.4 for heating services.

The tube-side convective heat transfer coefficient (ht) can be obtained by the definition of the Nusselt number

$$Nut = \frac{ht\ dti}{\widehat{kt}} \tag{15}$$

The pressure drop on the tube-side (ΔPt) is evaluated by the sum of the head losses in the tube bundle and in the front and rear headers

$$\frac{\Delta Pt}{\widehat{\rho t}\ \widehat{g}} = \frac{ft\ Npt\ L\ vt^2}{2\ \widehat{g}\ dti} + \frac{K\ Npt\ vt^2}{2\ \widehat{g}} \tag{16}$$

where ft is the tube-side friction factor and K is a parameter determined by the number of tube passes, it is equal to 0.9 for one tube pass and 1.6 for two or more.

The Darcy friction factor for turbulent flow is given by

$$ft = 0.014 + \frac{1.056}{Ret^{0.42}} \tag{17}$$

Overall heat-transfer coefficient

The overall heat-transfer coefficient (U) constraint is

$$U = \frac{1}{\frac{dte}{dti\ ht} + \frac{Rft\ dte}{dti} + \frac{dte\ln\left(\frac{dte}{dti}\right)}{2\ \widehat{ktube}} + \frac{1}{hs}} \tag{18}$$

where Rft is the fouling resistance in the tube side, the object of our modeling in the next section, and $\widehat{k\text{tube}}$ is the thermal conductivity of the tube wall.

Heat-transfer rate equation

This part of the model uses the LMTD method to develop the heat-transfer equation. This method is based on the logarithmic mean temperature difference ($\widehat{\Delta Tlm}$) that is described by

$$\widehat{\Delta Tlm} = \frac{\left(\widehat{Thi} - \widehat{Tco}\right) - \left(\widehat{Tho} - \widehat{Tci}\right)}{\ln\left(\frac{\left(\widehat{Thi} - \widehat{Tco}\right)}{\left(\widehat{Tho} - \widehat{Tci}\right)}\right)} \tag{19}$$

where $\widehat{Thi}$ and $\widehat{Tho}$ are the inlet and outlet temperatures of the hot stream, $\widehat{Tci}$ and $\widehat{Tco}$ are the inlet and outlet temperatures of the cold stream.

The heat-transfer rate equation constraint is

$$\widehat{Q} = U\ A\text{req}\ \widehat{\Delta Tlm}\ F \tag{20}$$

where $\widehat{Q}$ is the heat load, Areq is the required area, and F is the correction factor of the LMTD for encompassing multiple tube passes. The correction factor is equal to one if there is only one pass, otherwise, it is given by

$$F = \frac{\left(\widehat{R}^2 + 1\right)^{0.5}\ \ln\left(\frac{\left(1-\widehat{P}\right)}{\left(1-\widehat{R}\ \widehat{P}\right)}\right)}{\left(\widehat{R} - 1\right)\ln\left(\frac{2-\widehat{P}\left(\widehat{R}+1-\left(\widehat{R}^2+1\right)^{0.5}\right)}{2-\widehat{P}\left(\widehat{R}+1+\left(\widehat{R}^2+1\right)^{0.5}\right)}\right)} \tag{21}$$

where:

$$\widehat{R} = \frac{\widehat{Thi} - \widehat{Tho}}{\widehat{Tco} - \widehat{Tci}} \tag{22}$$

$$\widehat{P} = \frac{\widehat{Tco} - \widehat{Tci}}{\widehat{Thi} - \widehat{Tci}} \tag{23}$$

The heat-transfer area (A) is given by

$$A = Ntt\ \pi\ dte\ L \tag{24}$$

where Ntt is the total number of tubes.

Bounds on pressure drops, flow velocities, and Reynolds numbers

The pressure drop must be bounded in this model, as it is not included in the objective function

$$\Delta Ps \le \widehat{\Delta Psdisp} \tag{25}$$

$$\Delta Pt \le \widehat{\Delta Ptdisp} \tag{26}$$

Other variables that usually have upper and lower bounds are the velocities

$$\widehat{vsmin} \le vs \le \widehat{vsmax} \tag{27}$$

$$\widehat{vtmin} \le vt \le \widehat{vtmax} \tag{28}$$

The correlations used to calculate the heat-transfer coefficients impose the following validity ranges

$$Res \ge 2 \cdot 10^3 \tag{29}$$

$$Ret \ge 10^4 \tag{30}$$

Geometric constraints

In heat exchanger design, it is common to consider some constraints regarding relations between geometric variables. The baffle spacing must be limited between 20 and 100% of the shell diameter[22] and also the ratio between the tube length and shell diameter must be between 3 and 15[23]

$$lbc \geq 0.2\ Ds \tag{31}$$

$$lbc \leq 1.0\ Ds \tag{32}$$

$$L \geq 3\ Ds \tag{33}$$

$$L \leq 15\ Ds \tag{34}$$

Objective function

In heat exchanger design problems, it is common to have the minimization of the area as the goal, because it will impact directly in the cost of the heat exchanger. Therefore, in this work the objective function is

$$\min\ A \tag{35}$$

Threshold Fouling Models

Fouling in crude preheat trains can be associated to different mechanisms and the dominant effect depends on the position of the heat exchanger along the crude preheat train.[24] Upstream the desalter, fouling involves salt precipitation and the deposition of particulate matter. Downstream the desalter, as the temperature increases, chemical reaction fouling associated to the presence of asphaltenes becomes important. The deposition of corrosion products may occur along the entire train. The fouling problem at the fired heater occurs mainly due to coking.

This article is focused on the fouling problem at the hot end of the crude preheat train. These heat exchangers may be affected by higher fouling rates, and the reduction of the overall heat-transfer coefficient in these units has a direct impact in the energy recovery. The proposed analysis considers that only the crude oil stream is associated to a fouling rate.

Among the fouling modeling alternatives in the literature, the most common option employed in the high temperature heat exchangers in crude preheat trains is the utilization of threshold models. Threshold models are semiempirical models which describe the fouling rate as a balance between a formation rate and a suppression/removal rate. According to these models, higher temperatures and low velocities favor fouling. However, the combination of lower temperatures and higher velocities can suppress the fouling problem. Consequently, these models predict a threshold that delimits a "no fouling" region. The schematic representation of this region can be seen in Figure 1.

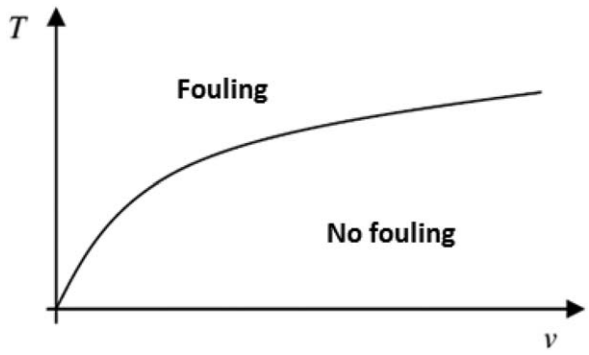

Figure 1. Threshold fouling.

The first threshold model was proposed by Ebert and Panchal[25]

$$\frac{dRf}{dt} = \alpha Re^{\beta} \exp\left(\frac{-Ea}{RT_f}\right) - \gamma \tau_w \tag{36}$$

where Re is the Reynolds number, T_f is the film temperature, R is the universal gas constant, τ_w is the shear stress, and α, β, γ, and Ea (activation energy) are empirical parameters. The empirical parameters must be determined based on laboratory or process data using a parameter estimation procedure and are specific for each crude.

Later, these authors proposed an extended version of the model[26]

$$\frac{dRf}{dt} = \alpha Re^{-0.66} Pr^{-0.33} \exp\left(\frac{-Ea}{RT_f}\right) - \gamma \tau_w \tag{37}$$

where Pr is the Prandtl number.

Polley et al.[27] proposed a modified model where the film temperature was substituted by the surface temperature and the shear stress was substituted by a Reynolds number-related term

$$\frac{dRf}{dt} = \alpha Re^{-0.8} Pr^{-0.33} \exp\left(\frac{-Ea}{RT_w}\right) - \gamma Re^{0.8} \tag{38}$$

A modification of the Polley et al.[27] model was proposed by Nasr and Givi[28]

$$\frac{dRf}{dt} = \alpha Re^{\beta} \exp\left(\frac{-Ea}{RT_f}\right) - \gamma Re^{0.4} \tag{39}$$

The models presented above can be used to describe the fouling rate in the tube-side flow, therefore, this assumption will be adopted in the optimization formulation. Reviews about threshold models with additional modeling alternatives can be found in Wilson et al.,[29,30] and Wang et al.[31]

The interpretation of the negative term in the threshold fouling model as suppression or removal is still in debate in the literature. The suppression hypothesis assumes that the thermofluid dynamic conditions may suppress the accumulation of deposits, but it cannot remove them once they are installed over the thermal surface, that is, according to this interpretation, the net fouling rate would be never negative (negative values predicted by the model would be overrun by zero).[32] The proposition of the optimization model developed in this article will not be affected by the difference between these two interpretations, therefore, we will identify this term from now on as "suppression," without loss of generality.

Analysis of Fouling

The aggregation of the relation between the fouling resistance and the thermofluid dynamic conditions in the heat exchanger allows the optimization model to find design alternatives where the reduction of the fouling rate implies a higher overall heat-transfer coefficient and, consequently, a smaller heat-transfer area. We explored the impact of this using a fouling resistance model in relation to the flow velocity in Lemos et al.[18]

The analysis of the threshold models allows to identify a set of conditions associated to the fouling resistance that can be accommodated in the optimal design formulation. These conditions are discussed below based on the Polley et al.[27] model. Similar analysis can be applied to the other threshold models. The fluid dynamic impact of fouling is not contemplated in the current analysis.

Model structure

The fouling rate expression and the threshold conditions depend on the surface temperature. At the clean condition, this temperature corresponds to the tube wall inner surface temperature. After the deposit accumulation, it is possible to consider that this temperature becomes the temperature of the interface between the fluid and the deposit. Therefore, a more compact representation of Polley et al.[27] model using the surface temperature (T_s) is given by

$$\frac{dRf}{dt} = \widehat{Af} Re^{-0.8} \exp\left(\frac{-\widehat{\psi f}}{T_s}\right) - \widehat{Bf} Re^{0.8} \tag{40}$$

where

$$\widehat{Af} = \alpha \ Pr^{-0.33} \tag{41}$$

$$\widehat{Bf} = \gamma \tag{42}$$

$$\widehat{\psi f} = \frac{-Ea}{R} \tag{43}$$

The terms in the right-hand side of Eq. 40 are the formation rate (FR) and the suppression rate (SR)

$$FR = \widehat{Af} Re^{-0.8} \exp\left(\frac{-\widehat{\psi f}}{T_s}\right) \tag{44}$$

$$SR = \widehat{Bf} Re^{0.8} \tag{45}$$

Therefore, the threshold condition ($FR = SR$) is

$$\widehat{Af} Re^{-0.8} \exp\left(\frac{-\widehat{\psi f}}{T_s}\right) = \widehat{Bf} Re^{0.8} \tag{46}$$

where this equation means that when the formation rate and the suppression rate are equal, the fouling resistance value will correspond to the asymptotic fouling resistance, that will be used later in the development.

The evaluation of the surface temperature is based on the thermal circuit between the hot and cold streams depicted in Figure 2

$$\frac{\widehat{Th} - Ts}{\frac{1}{hs} + \frac{dte \ \ln(dte/dti)}{2\widehat{k\text{tube}}} + Rft\left(\frac{dte}{dti}\right)} = \frac{Ts - \widehat{Tc}}{\frac{1}{ht}\left(\frac{dte}{dti}\right)} \tag{47}$$

Isolating Ts from the expression, it yields

$$Ts = \frac{\left(\widehat{Th} - \widehat{Tc}\right)\frac{1}{h_t}\frac{dte}{dti}}{\frac{1}{hs} + \frac{dte \ \ln(dte/dti)}{2\widehat{k\text{tube}}} + \frac{1}{ht}\left(\frac{dte}{dti}\right) + Rft\left(\frac{dte}{dti}\right)} + \widehat{Tc} \tag{48}$$

This equation can be expressed in a more compact form using the overall heat-transfer coefficient at a clean condition (Uc)

$$Ts = \frac{\left(\widehat{Th} - \widehat{Tc}\right)\frac{1}{h_t}\frac{dte}{dti}}{\frac{1}{Uc} + Rf\left(\frac{dte}{dti}\right)} + \widehat{Tc} \tag{49}$$

The heat transfer along the thermal surface implies that $\widehat{Th}$ and $\widehat{Tc}$ vary. Because the design procedure does not rely on local temperatures and properties (they are not modeled), but rather on average values, we need to rely on average values as well. Therefore, we assume average values to apply this equation to the entire equipment

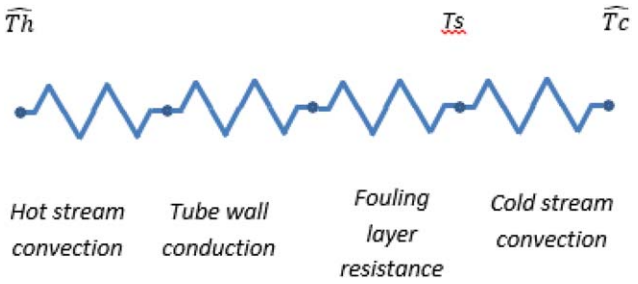

Figure 2. Thermal circuit between hot and cold streams.

[Color figure can be viewed at wileyonlinelibrary.com]

$$Ts = \frac{\widehat{\Delta T}^{av}\frac{1}{h_t}\frac{dte}{dti}}{\frac{1}{Uc} + Rf\left(\frac{dte}{dti}\right)} + \widehat{Tc}^{av} \tag{50}$$

The extreme values that the surface temperature can reach will be important in the analysis of the fouling condition in the design, because they are associated to the limiting values of the formation rate (higher surface temperatures implies higher formation rates).

The highest value of the surface temperature occurs at the clean condition (e.g., $Rf = 0$ at the start-up)

$$Ts_{\max} = \frac{\widehat{\Delta T}^{av}\frac{1}{h_t}\frac{dte}{dti}}{\frac{1}{Uc}} + \widehat{Tc}^{av} \tag{51}$$

The corresponding maximum fouling formation rate (FR) becomes

$$FR_{\max} = \widehat{Af} Re^{-0.8} \exp\left(\frac{-\widehat{\psi f}}{\frac{\widehat{\Delta T}^{av}\frac{1}{h_t}\frac{dte}{dti}}{\frac{1}{Uc}} + \widehat{Tc}^{av}}\right) \tag{52}$$

The lowest value that the surface temperature can reach is the cold stream temperature

$$Ts_{\min} = \widehat{Tc}^{av} \tag{53}$$

The corresponding fouling formation rate becomes

$$FR_{\min} = \widehat{Af} Re^{-0.8} \exp\left(\frac{-\widehat{\psi f}}{\widehat{Tc}^{av}}\right) \tag{54}$$

The following subsections explore the three fouling conditions employed in the formulation of the design optimization: no fouling condition, fouling continuous growth, and asymptotic fouling resistance.

No fouling condition

If the suppression rate is higher than the formation rate at the clean condition (that it is the condition of the highest formation rate), then the fouling rate will be always equal to zero and no fouling layer will be formed.

The mathematical expression of the no fouling condition is

$$FR_{\max} \leq SR \tag{55}$$

This condition must be associated to a null fouling resistance in the design procedure

$$Rft = 0 \tag{56}$$

Fouling condition: Continuous growth

If the formation rate is higher than the suppression rate, then a fouling layer will be formed over the thermal surface. In this case, the following mathematical relation holds

$$FR_{\max} > SR \tag{57}$$

The growth of the fouling layer reduces the surface temperature gradually and consequently, the fouling rate reduces due to the decrease of the formation rate. However, instead of considering that one allows reaching a value equivalent to the suppression rate (i.e., zero fouling rate condition), the formation rate can be limited by a constant value higher than the suppression rate. This condition is identified by

$$FR_{\min} > SR \tag{58}$$

As, in this condition, the fouling resistance always increases, the design procedure can adopt a maximum fouling resistance previously established

$$Rft = \widehat{Rf}^{\max} \tag{59}$$

Fouling condition: Asymptotic resistance

Differently from the previous condition, the fouling growth can reduce the formation rate until it reaches the suppression rate. In this case, the fouling resistance assumes an asymptotic value. The corresponding mathematical condition is

$$FR_{\min} \leq SR \tag{60}$$

The corresponding value of the asymptotic fouling resistance (Rf^{∞}) in this situation can be obtained by the root of Eq. 46 in relation to Rf from Eq. 49, as follows

$$Rf^{\infty} = \frac{\widehat{\Delta T}^{av}\left(\frac{1}{h_t}\right)}{\left[\frac{\widehat{\psi f}}{\ln\left(\frac{\widehat{Af}\ \widehat{Ret}^{-1.6}}{\widehat{Bf}}\right)}\right]} - \frac{1}{Uc}\frac{dti}{dte} - \widehat{Tc}^{av} \tag{61}$$

Aiming at the design problem, the fouling resistance value to be adopted in the design solution procedure must be the lowest value between the asymptotic fouling resistance and the maximum value imposed by the designer

$$Rft = \min\left(\widehat{Rf}^{\max}, Rf^{\infty}\right) \tag{62}$$

Fluid dynamic impact of fouling

The growth of the fouling layer would also have a fluid dynamic impact that is not included in our model, where the Reynolds number is always calculated using the clean inner tube diameter.

The increase of the fouling layer reduces the cross-sectional area and, consequently, there is an increase of the flow velocity and Reynolds number that causes an increase of the suppression rate. Considering the fouling condition associated to a continuous growth discussed above, the inclusion of the fluid dynamic fouling impact would be able to identify an equilibrium between suppression and formation rates that cannot be captured mathematically by the model proposed in this article. In a similar way, in the fouling condition associated to an asymptotic resistance, the fluid dynamic modeling would imply a reduction of the fouling resistance due to the increase of the velocity. Nevertheless, the solution proposed here is conservative, always providing a feasible design. Future work will handle this situation better.

Table 1. Propositions and Corresponding Binary Variables

Proposition	Binary Variable
$FR_{\max} \leq SR$	y_1
$FR_{\min} \leq SR$	y_2
$\boldsymbol{Rf^{\infty} \leq \widehat{Rf}^{\max}}$	y_3

Binary representation of the fouling conditions

The three fouling conditions identified above can be inserted into the optimization model by a set of binary variables related to a corresponding set of propositions, as shown in Table 1 (if the proposition is true, the corresponding binary variable is equal to 1).

The mathematical relations among the binary variables and the corresponding propositions are

$$\widehat{L1}\ y1 + \varepsilon \leq FR_{\max} - SR \leq \widehat{U1}\ (1 - y1) \tag{63}$$

$$\widehat{L2}\ y2 + \varepsilon \leq FR_{\min} - SR \leq \widehat{U2}\,(1 - y2) \tag{64}$$

$$\widehat{L3}\ y3 + \varepsilon \leq Rf^{\infty} - \widehat{Rf}^{\max} \leq \widehat{U3}\,(1 - y3) \tag{65}$$

where ε is a small positive number, $\widehat{U1}$ and $\widehat{L1}$ are upper and lower bounds for the difference $FR_{\max} - SR$, $\widehat{U2}$ and $\widehat{L2}$ are upper and lower bounds for the difference $FR_{\min} - SR$, and $\widehat{U3}$ and $\widehat{L3}$ are upper and lower bounds for the difference $Rf^{\infty} - \widehat{Rf}^{\max}$.

Based on this set of binary variables, each of the fouling conditions is identified by a certain combination of 0–1 values, as shown in Table 2.

The different combinations of values of the binary variables can be organized for the evaluation of the fouling resistance according to each condition identified in Table 2

$$\begin{aligned} Rft = {} & y3\ Rf^{\infty} - Rf^{\infty} + y2\ Rf^{\infty} - y1\ Rf^{\infty} \\ & + (1 - y2 + 1 - y3)\ \widehat{Rf}^{\max} \end{aligned} \tag{66}$$

MILP Model

This section presents the development of a linear formulation for the optimization of the design of shell-and-tube heat exchangers considering the threshold model discussed above. The approach employed is based on the methodology described by Gonçalves et al.[11]

Table 2. Relation Among the Binary Variables and the Fouling Conditions

Variable	No Fouling	Continuous Fouling Growth	Asymptotic Resistance with $Rf^{\infty} \leq \widehat{Rf}^{\max}$	Asymptotic Resistance with $Rf^{\infty} > \widehat{Rf}^{\max}$
y1	1	0	0	0
y2	1	0	1	1
y3	1	1	1	0
Rft	0	$\widehat{Rf}^{\max}$	$\widehat{Rf}^{\infty}$	$\widehat{Rf}^{\max}$

Discrete design variables

The geometric variables of the heat exchanger design are available in standard/commercial values. Therefore, they can be represented by a set of binary variables

$$dte = \sum_{sd=1}^{sd\max} \widehat{pdte}_{sd}\ yd_{sd} \tag{67}$$

$$dti = \sum_{sd=1}^{sd\max} \widehat{pdti}_{sd}\ yd_{sd} \tag{68}$$

$$Ds = \sum_{sDs=1}^{sDs\max} \widehat{pDs}_{sDs}\ yDs_{sDs} \tag{69}$$

$$\text{lay} = \sum_{slay=1}^{slay\max} \widehat{p\text{lay}}_{slay}\ y\text{lay}_{slay} \tag{70}$$

$$Npt = \sum_{sNpt=1}^{sNpt\max} \widehat{pNpt}_{sNpt}\ yNpt_{sNpt} \tag{71}$$

$$rp = \sum_{srp=1}^{srp\max} \widehat{prp}_{srp} yrp_{srp} \tag{72}$$

$$L = \sum_{sL=1}^{sL\max} \widehat{pL}_{sL}\ yL_{sL} \tag{73}$$

$$Nb = \sum_{sNb=1}^{sNb\max} \widehat{pNb}_{sNb}\ yNb_{sNb} \tag{74}$$

where *dte*, *dti*, *Ds*, lay, *Npt*, *rp*, *L*, and *Nb* are the inner and outer tube diameters, shell diameter, tube layout (square or triangular), number of tube passes, pitch ratio, tube length, and number of baffles; $\widehat{pdte}$, $\widehat{pdti}$, $\widehat{pDs}$, $\widehat{pNpt}$, $\widehat{prp}$, $\widehat{play}$, $\widehat{pL}$, and $\widehat{pNb}$ are the corresponding set of discrete values for each variable; and *yd*, *yDs*, *y*lay, *yNpt*, *yrp*, *yL*, and *yNb* are the corresponding binary variables that express the selection of a given standard alternative. As only one alternative can be chosen, the following constraints must be included

$$\sum_{sd=1}^{sd\max} yd_{sd} = 1 \tag{75}$$

$$\sum_{sDs=1}^{sDs\max} yDs_{sDs} = 1 \tag{76}$$

$$\sum_{slay=1}^{slay\max} y\text{lay}_{slay} = 1 \tag{77}$$

$$\sum_{sNpt=1}^{sNpt\max} yNpt_{sNpt} = 1 \tag{78}$$

$$\sum_{srp=1}^{srp\max} yrp_{srp} = 1 \tag{79}$$

$$\sum_{sL=1}^{sL\max} yL_{sL} = 1 \tag{80}$$

$$\sum_{sNb=1}^{sNb\max} yNb_{sNb} = 1 \tag{81}$$

To minimize the computational effort, the set of geometric variables can be reorganized using a unique set of binaries associated to a multi-index *s*row = (*sd, sDs, s*lay*, sNpt, srp, sL, sNb*). Therefore, the available values of the discrete variables assume the following representation

$$\widehat{Pdte}_{s\text{row}} = \widehat{pdte}_{sd} \tag{82}$$

$$\widehat{Pdti}_{s\text{row}} = \widehat{pdti}_{sd} \tag{83}$$

$$\widehat{PDs}_{s\text{row}} = \widehat{pDs}_{sDs} \tag{84}$$

$$\widehat{Play}_{s\text{row}} = \widehat{play}_{s\text{lay}} \tag{85}$$

$$\widehat{PNpt}_{s\text{row}} = \widehat{pNpt}_{sNpt} \tag{86}$$

$$\widehat{Prp}_{s\text{row}} = \widehat{prp}_{srp} \tag{87}$$

$$\widehat{PL}_{s\text{row}} = \widehat{pL}_{sL} \tag{88}$$

$$\begin{array}{cccccccc}
\widehat{Pdte}_1 & \widehat{Pdti}_1 & \widehat{PDs}_1 & \ldots & \ldots & \ldots & \widehat{PL}_1 & \widehat{PNb}_1 \\
\widehat{Pdte}_1 & \widehat{Pdti}_1 & \widehat{PDs}_1 & \ldots & \ldots & \ldots & \widehat{PL}_1 & \widehat{PNb}_2 \\
\widehat{Pdte}_1 & \widehat{Pdti}_1 & \widehat{PDs}_1 & \cdots & \ldots & \ldots & \widehat{PL}_1 & \widehat{PNb}_3 \\
\vdots & \vdots & \vdots & \ddots & & & & \\
\vdots & \vdots & \vdots & & \ddots & & \vdots & \vdots \\
\vdots & \vdots & \vdots & & & \ddots & & \\
\widehat{Pdte}_{n-1} & \widehat{Pdti}_{n-1} & \widehat{PDs}_n & \ldots & \ldots & \ldots & \widehat{PL}_n & \widehat{PNb}_n \\
\widehat{Pdte}_n & \widehat{Pdti}_n & \widehat{PDs}_n & \ldots & \ldots & \cdots & \widehat{PL}_n & \widehat{PNb}_n
\end{array}$$

Figure 3. Tabular organization of the discrete values of the geometric variables.

$$\widehat{PNb}_{s\text{row}} = \widehat{pNb}_{sNb} \tag{89}$$

According to this representation, the available options of the discrete variables are grouped in a tabular structure, where each row corresponds to a candidate heat exchanger, as illustrated by Figure 3.

Therefore, the space of design alternatives is described by a single set of binary variables

$$dte = \sum_{s\text{row}} \widehat{Pdte}_{s\text{row}}\ y\text{row}_{s\text{row}} \tag{90}$$

$$dti = \sum_{s\text{row}} \widehat{Pdti}_{s\text{row}}\ yrow_{s\text{row}} \tag{91}$$

$$Ds = \sum_{s\text{row}} \widehat{PDs}_{s\text{row}}\ yro\text{w}_{s\text{row}} \tag{92}$$

$$\text{lay} = \sum_{s\text{row}} \widehat{P\text{lay}}_{s\text{row}}\ y\text{row}_{s\text{row}} \tag{93}$$

$$Npt = \sum_{s\text{row}} \widehat{PNpt}_{s\text{row}}\ y\text{row}_{s\text{row}} \tag{94}$$

$$rp = \sum_{s\text{row}} \widehat{Prp}_{s\text{row}} y\text{row}_{s\text{row}} \tag{95}$$

$$L = \sum_{s\text{row}} \widehat{PL}_{s\text{row}}\ y\text{row}_{s\text{row}} \tag{96}$$

$$Nb = \sum_{s\text{row}} \widehat{PNb}_{s\text{row}}\ y\text{row}_{s\text{row}} \tag{97}$$

$$\sum_{s\text{row}} y\text{row}_{s\text{row}} = 1 \tag{98}$$

Reformulation to a linear model

The original nonlinear constraints described in Eqs. 1–35 are reformulated by substituting the geometric variables expressed through their corresponding binary representation described in Eqs. 90–97. The nature of the binary variables and the mathematical structure of the constraints imply that these substitutions can be manipulated to obtain linear constraints, as shown below. It is important to highlight that this procedure is not a linearization, in the sense of an approximate solution, but a rigorous reformulation, it transforms the original problem into a linear one. Therefore, the solutions of one, are exactly the solutions of the other, with the exception that the former is nonlinear and can give local optima (except when run by a global optimizer), and the latter, being linear is globally optimal.

The problem constraints ($h(dte, dti, \ldots, Nb)$) are composed by expressions involving products of powers, such as

$$h(dte, dti, \ldots, Nb) = K\ dte^{n1} dti^{n2} \cdots Nb^{n8} \tag{99}$$

where *K* is a model constant.

The substitution of the binary representation of the geometric variables yields

$$h(\text{yrow}_{srow}) = K \left[\sum_{srow} \widehat{Pdte}_{srow}\ \text{yrow}_{srow}\right]^{n1} \left[\sum_{srow} \widehat{Pdti}_{srow}\ \text{yrow}_{srow}\right]^{n2} \ldots \left[\sum_{srow} \widehat{PNb}_{srow}\ \text{yrow}_{srow}\right]^{n8} \tag{100}$$

Because all binary variables are equal to 1 only once in the corresponding set, this equation is equivalent to

$$h(\ \text{yrow}_{srow}) = K\ \sum_{srow} \widehat{Pdte}_{srow}^{n1} \widehat{Pdti}_{srow}^{n2} \ldots \widehat{PNb}_{srow}^{n8}\ \text{yrow}_{srow} \tag{101}$$

The application of this procedure to all constraints results in a set of linear relations only involving binary variables. The details of all expressions of the linear model for the design of heat exchangers can be found in Gonçalves et al.[11] and will not be repeated here (the on-line Supporting Information contains the entire mixed-integer linear formulation encompassing all constraints). The next subsection will explore how this model can be extended to accommodate the fouling threshold model.

Extension to include the threshold fouling modeling

The interconnection of the fouling threshold model and the formulation of the heat exchanger design optimization is the heat-transfer rate equation, where the fouling resistance is present. According to Gonçalves et al.,[11] this expression is given by

$$\widehat{Q}\left(\sum_{srow} \frac{\widehat{Pdte}_{srow}}{\widehat{Pht}_{srow}\ \widehat{Pdti}_{srow}} \text{yrow}_{srow} + \sum_{srow} \frac{\widehat{Pdte}_{srow}}{\widehat{Pdti}_{srow}} \widehat{Rft}\ \text{yrow}_{srow} + \frac{\sum_{srow} \widehat{Pdte}_{srow}\ \text{yrow}_{srow} \ln\left(\frac{\widehat{Pdte}_{srow}}{\widehat{Pdti}_{srow}}\right)}{2\ \widehat{ktube}} + \sum_{srow} \frac{1}{\widehat{Phs}_{srow}} \text{yrow}_{srow}\right) \leq \left(\frac{100}{100+\widehat{Aexc}}\right)\left(\pi \sum_{srow} \widehat{PNtt}_{srow}\ \widehat{Pdte}_{srow}\ \widehat{PL}_{srow} yrow_{srow}\right) \widehat{\Delta Tlm}\ \widehat{F}_{srow} \tag{102}$$

In the case discussed by Gonçalves et al.,[11] the fouling resistance is a parameter ($\widehat{Rft}$).

In our proposed approach, the fouling resistance is a variable

$$\widehat{Q}\left(\sum_{srow} \frac{\widehat{Pdte}_{srow}}{\widehat{Pht}_{srow}\ \widehat{Pdti}_{srow}} \text{yrow}_{srow} + \sum_{srow} \frac{\widehat{Pdte}_{srow}}{\widehat{Pdti}_{srow}} Rft\ \text{yrow}_{srow} + \frac{\sum_{srow} \widehat{Pdte}_{srow}\ \text{yrow}_{srow} \ln\left(\frac{\widehat{Pdte}_{srow}}{\widehat{Pdti}_{srow}}\right)}{2\ \widehat{k\text{tube}}} + \sum_{srow} \frac{1}{\widehat{Phs}_{srow}} \text{yrow}_{srow}\right) \leq \left(\frac{100}{100+\widehat{Aexc}}\right)\left(\pi \sum_{srow} \widehat{PNtt}_{srow}\ \widehat{Pdte}_{srow}\ \widehat{PL}_{srow} \text{yrow}_{srow}\right) \widehat{\Delta Tlm}\ \widehat{F}_{srow} \tag{103}$$

Now, this constraint contains a bilinear term resultant from the product of the fouling resistance and the design binary variable ($Rft\ \text{yrow}_{srow}$). This nonlinearity can be eliminated replacing it by a new variable wRf_{srow}, together with the insertion of additional constraints,[33] as follows

$$\widehat{Q}\left(\sum_{srow} \frac{\widehat{Pdte}_{srow}}{\widehat{Pht}_{srow}\ \widehat{Pdti}_{srow}} \text{yrow}_{srow} + \sum_{srow} \frac{\widehat{Pdte}_{srow}}{\widehat{Pdti}_{srow}} wRf_{srow} + \frac{\sum_{srow} \widehat{Pdte}_{srow}\ \ln\left(\frac{\widehat{Pdte}_{srow}}{\widehat{Pdti}_{srow}}\right)\ \text{yrow}_{srow}}{2\ \widehat{k\text{tube}}} + \sum_{srow} \frac{1}{\widehat{Phs}_{srow}} \text{yrow}_{srow}\right) \leq \left(\frac{100}{100+\widehat{Aexc}}\right)\left(\pi \sum_{srow} \widehat{PNtt}_{srow}\ \widehat{Pdte}_{srow}\ \widehat{PL}_{srow} \text{yrow}_{srow}\right) \widehat{\Delta Tlm}\ \widehat{F}_{srow} \tag{104}$$

$$\widehat{LRf} \leq Rft \leq \widehat{URf} \tag{105}$$

$$Rft - \widehat{URf}(1-\text{yrow}_{srow}) \leq wRf_{srow} \leq Rft - \widehat{LRf}(1-\text{yrow}_{srow}) \tag{106}$$

$$\widehat{LRf}\ \text{yrow}_{srow} \leq wRf_{srow} \leq \widehat{URf}\ \text{yrow}_{srow} \tag{107}$$

There are also nonlinearities in Eq. 66 that are treated in the same way, replacing them by $w1Rf^{\infty}$, $w2Rf^{\infty}$, and $w3Rf^{\infty}$, respectively

$$Rft = w3Rf^{\infty} - Rf^{\infty} + w2Rf^{\infty} - w1Rf^{\infty} + (1-y2+1-y3)\ \widehat{Rf}^{\max} \tag{108}$$

$$\widehat{LRfinf} \leq Rf^{\infty} \leq \widehat{URfinf} \tag{109}$$

Table 3. Physical Properties

	Density (kg/m^3)	Viscosity (Pa·s)	Conductivity (W/m·K)	Heat Capacity (J/kgK)
Cold stream	768.9	$5.36\cdot10^{-4}$	0.09	2742.5
Hot stream	898.0	$1.87\cdot10^{-3}$	0.13	2754.0

Table 4. Thermal Service

	Cold Stream	Hot Stream
Mass flow rate (kg/s)	91.9	40.0
Inlet temperature (°C)	288.4	343.8
Outlet temperature (°C)	305.0	305.4
Maximum pressure drop (kPa)	80	80
Flow velocity bounds (m/s)	1.0–3.0	0.5–2.0

$$Rf^{\infty}-\widehat{URfinf}(1-y1)\le w1Rf^{\infty}\le Rf^{\infty}-\widehat{LRfinf}(1-y1) \tag{110}$$

$$\widehat{LRfinf}\ \ y1\le w1Rf^{\infty}\le \widehat{URfinf}\ \ y1 \tag{111}$$

$$Rf^{\infty}-\widehat{URfinf}(1-y2)\le w2Rf^{\infty}\le Rf^{\infty}-\widehat{LRfinf}(1-y2) \tag{112}$$

$$\widehat{LRfinf}\ \ y2\le w2Rf^{\infty}\le \widehat{URfinf}\ \ y2 \tag{113}$$

$$Rf^{\infty}-\widehat{URfinf}(1-y3)\le w3Rf^{\infty}\le Rf^{\infty}-\widehat{LRfinf}(1-y3) \tag{114}$$

$$\widehat{LRfinf}\ \ y3\le w3Rf^{\infty}\le \widehat{URfinf}\ \ y3 \tag{115}$$

The terms SR (Eq. 45), $FR_{\max}$ (Eq. 52), $FR_{\min}$ (Eq. 54), and Rf^{∞} (Eq. 61) are also reformulated by the substitution of the binary variables

$$SR=\widehat{Bf}\left(\frac{4\ \widehat{mt}}{\pi\ \widehat{\mu t}}\right)^{0.8}\sum_{srow}\left(\frac{\widehat{PNpt}_{srow}}{\widehat{PNtt}_{srow}\ \widehat{Pdti}_{srow}}\right)^{0.8}\text{yrow}_{srow} \tag{116}$$

$$FR_{\max}=\widehat{Af}\left(\frac{4\ \widehat{mt}}{\pi\ \widehat{\mu t}}\right)^{-0.8}\sum_{srow}\left(\frac{\widehat{PNpt}_{srow}}{\widehat{PNtt}_{srow}\ \widehat{Pdti}_{srow}}\right)^{-0.8}$$
$$\exp\left(\frac{-\widehat{\psi f}}{\widehat{Tc}^{av}+\left[\frac{\widehat{\Delta T}^{av}\ \frac{\widehat{pdte}_{srow}}{\widehat{pht}_{srow}\ \widehat{pdti}_{srow}}}{\frac{\widehat{Pdte}_{srow}}{\widehat{Pht}_{srow}\ \widehat{Pdti}_{srow}}+\frac{\widehat{Pdte}_{srow}\ln\left(\frac{\widehat{Pdte}_{srow}}{\widehat{Pdti}_{srow}}\right)}{2\ \widehat{k\text{tube}}}+\frac{1}{\widehat{Phs}_{srow}}}\right]}\right)\text{yrow}_{srow} \tag{117}$$

$$FR_{\min}=\widehat{Af}\left(\frac{4\ \widehat{mt}}{\pi\ \widehat{\mu t}}\right)^{-0.8}\exp\left(\frac{-\widehat{\psi}}{\widehat{Tc}^{av}}\right)\sum_{srow}\left(\frac{\widehat{PNpt}_{srow}}{\widehat{PNtt}_{srow}\ \widehat{Pdti}_{srow}}\right)^{-0.8}\text{yrow}_{srow} \tag{118}$$

$$Rf^{\infty}=\sum_{srow}\frac{\widehat{\Delta T}^{av}/\widehat{pht}_{srow}}{\left[\frac{\widehat{\psi f}}{\ln\left[\frac{\widehat{Af}\left(\frac{\widehat{4mt}}{\pi\mu t\ PNtt_{srow}}\ \frac{\widehat{PNpt}_{srow}}{Pdti_{srow}}\right)^{-(1.6)}}{\widehat{Bf}}\right]}-\widehat{Tc}^{av}\right]}\text{yrow}_{srow}$$
$$-\sum_{srow}\left[\frac{\widehat{Pdti}_{srow}}{\widehat{Pdte}_{srow}}\left(\frac{\widehat{Pdte}_{srow}}{\widehat{Pht}_{srow}\ \widehat{Pdti}_{srow}}+\frac{\widehat{Pdte}_{srow}\ln\left(\frac{\widehat{Pdte}_{srow}}{\widehat{Pdti}_{srow}}\right)}{2\ \widehat{k\text{tube}}}+\frac{1}{\widehat{Phs}_{srow}}\right)\right]\text{yrow}_{srow} \tag{119}$$

Table 5. Alternatives of Discrete Values of the Geometric Variables

Variable	Values
Tube outer diameter, $\widehat{pdte}_{sd}$ (m)	0.01905, 0.02540, 0.03175, 0.03810, 0.05080
Tube inner diameter, $\widehat{pdti}_{sd}$(m)	0.01575, 0.02210, 0.02845, 0.03480, 0.04750
Tube length, $\widehat{pL}_{sL}$ (m)	1.2195, 1.8293, 2.4390, 3.0488, 3.6585, 4.8768, 6.0976
Number of baffles, $\widehat{pNb}_{sNb}$	1, 2, …, 20
Number of tube passes, $\widehat{pNpt}_{sNpt}$	1, 2, 4, 6
Tube pitch ratio, $\widehat{prp}_{srp}$	1.25, 1.33, 1.50
Shell diameter, $\widehat{pDs}_{sDs}$ (m)	0.7874, 0.8382, 0.889, 0.9398, 0.9906, 1.0668, 1.143, 1.2192, 1.3716, 1.524
Tube layout, $\widehat{play}_{slay}$	1 = square, 2 = triangular

Table 6. Parameters of the Fouling Model

α (m^2K/J)	γ (m^2K/J)
0.2798	$4.17 \cdot 10^{-13}$

Table 7. Results for Example 1—Design Variables

Variable	Value	Variable	Value
A (m^2)	585	rp	1.25
dte (m)	0.0254	Ds (m)	1.22
dti (m)	0.0221	lay	2
L (m)	6.10	ltp (m)	0.0317
Nb	19	Ntt	1203
Npt	6	ebc (m)	0.305

Finally, the set of constraints to include the threshold model in the formulation of the heat exchanger design optimization encompasses the constraints regarding the heat-transfer rate equation (Eqs. 104–107), the fouling resistance evaluation (Eqs. 108–115), and fouling conditions (Eqs. 63–65 and Eqs. 116–119).

Results

Three examples are used to illustrate the differences of our proposed approach as compared to the use of recommended fixed fouling resistances. These examples explore different situations involving a no fouling case, the fouling resistance equal to $\widehat{Rf}^{MAX}$, and the fouling resistance equal to Rf^{∞}. In addition, three case studies are also presented considering the relation between the heat exchanger design and fouling aspects, involving crude oil type, pressure drop manipulation, and energy integration.

Table 3 presents the physical properties of the streams, associated to average values calculated along the temperature operating range, and Table 4 displays the characteristics of the thermal service. These values are taken from a real preheat train, where the hot stream flows in the shell-side and the cold stream, crude oil, flows in the tubes. The discrete values used as parameters related to the geometric variables are present in Table 5. The thermal conductivity of the tube wall is equal to 50 W/m·K.

The fouling resistance used for the traditional approach is $7.04 \cdot 10^{-4}$ m^2K/W, which corresponds to the TEMA indication[12] for the crude oil flowing in the conditions depicted in Table 4. This value will be also used as the maximum fouling resistance in the proposed design procedure ($\widehat{Rf}^{MAX}$).

The values of the empirical parameters of the fouling rate model are displayed in Table 6, close to the values reported by Polley et al.,[34] with the exception of the activation energy that was modified in each example so that all the three different possibilities could be achieved through the same service. The identification of fouling model parameters can be conducted using a parameter estimation procedure based on laboratory or process data.[34–36]

The computational time, which corresponds to the elapsed time using a computer with Intel Core i7 processor with 8 Mb of RAM memory, was less than 40 seconds to all of the examples and case studies displayed here.

Example 1

The results obtained using the proposed approach for an activation energy of 40,000 J/mol are displayed in Tables 7 and 8.

This case leads to a fouling resistance value that is equal to $\widehat{Rf}^{MAX}$, which means that the design fouling resistance will be the same proposed by TEMA. In this particular scenario, the results obtained by the proposed approach are exactly the same as the ones obtained with the traditional approach, as the fouling resistance values are the same.

Example 2

The results obtained for the proposed approach with an activation energy of 41,000 J/mol are displayed in Tables 9 and 10.

The proposed approach leads to a solution associated to an asymptotic fouling resistance (Rf^{∞}) equal to $3.22 \cdot 10^{-5}$ m^2K/W, lower than the value adopted by TEMA ($7.04 \cdot 10^{-4}$ m^2K/W). Therefore, the proposed design procedure could identify an alternative associated to a smaller fouling resistance and, consequently, with a smaller area. Indeed, our optimal heat exchanger has an area of 412 m^2 and the corresponding result with the TEMA fixed fouling resistance (shown in Example 1) is 585 m^2, that is, the optimization could achieve a reduction in the heat-transfer area of 29%.

Example 3

In this last example, the value of the activation energy is 48,000 J/mol. The corresponding optimization results are displayed in Tables 11 and 12.

This case leads to a no fouling condition, which allowed a considerable increase of the overall heat-transfer coefficient, and consequently, a reduction of the heat transfer area.

Table 8. Results for Example 1—Thermofluid Dynamic Variables

Variable	Value
ΔPs (Pa)	74001
ΔPt (Pa)	47833
hs (W/m^2K)	984
ht (W/m^2K)	1638
U (W/m^2K)	390
vs (m/s)	0.60
vt (m/s)	1.55

Table 9. Results for Example 2—Design Variables

Variable	Value	Variable	Value
A (m^2)	412	rp	1.25
dte (m)	0.03175	Ds (m)	1.14
dti (m)	0.02845	lay	2
L (m)	6.10	ltp (m)	0.0397
Nb	17	Ntt	677
Npt	6	ebc (m)	0.339

Table 10. Results for Example 2 – Thermofluid Dynamic Variables

Variable	Value
ΔPs (Pa)	44483
ΔPt (Pa)	43046
hs (W/m^2K)	870
ht (W/m^2K)	1646
U (W/m^2K)	527
vs (m/s)	0.58
vt (m/s)	1.67

Table 11. Results for Example 3—Design Variables

Variable	Value	Variable	Value
A (m^2)	321	rp	1.25
dte (m)	0.01905	Ds (m)	0.940
dti (m)	0.01575	lay	1
L (m)	4.88	ltp (m)	0.02381
Nb	15	Ntt	1100
Npt	4	ebc (m)	0.305

Table 12. Results for Example 3—Thermofluid Dynamic Variables

Variable	Value
ΔPs (Pa)	70706
ΔPt (Pa)	71992
hs (W/m^2K)	1121
ht (W/m^2K)	2340
U (W/m^2K)	692
vs (m/s)	0.78
vt (m/s)	2.23

Comparing with the traditional approach, this solution allowed a reduction of 45% in the heat exchanger area.

The no fouling behavior can be illustrated by the envelope of fouling threshold (Eq. 46) represented in Figure 4, where it can be observed the position corresponding to the optimal heat exchanger inside the no fouling region.

Case study 1: Crude oil selection

Different crudes can be more or less prone to fouling. The introduction of fouling modeling in the heat exchanger design procedure can bring a better understanding of the impact of the crude oil selection on the design of the crude preheat train.

Example 3 showed a crude oil associated to an activation energy of 48,000 J/mol that was associated to an optimal exchanger with a heat transfer area of 321 m^2 and no fouling behavior. The utilization of an alternative crude oil with activation energy of 43,000 J/mol would imply that the previous optimal solution would not be feasible anymore. The application of the design procedure finds a solution in this new condition associated to an increase of the heat transfer area of 8%, according to the solution depicted in Tables 13 and 14. This solution alternative is inside the no fouling region of the alternative crude oil stream, but the original heat exchanger would be located outside the no fouling envelope.

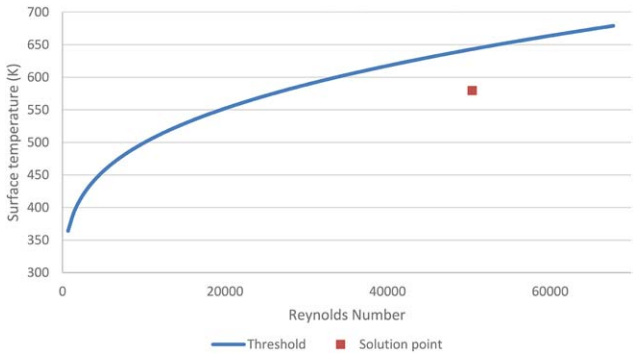

Figure 4. Example 3: Threshold fouling and optimal heat exchanger solution.

[Color figure can be viewed at wileyonlinelibrary.com]

Table 13. Results for Case Study 1—Design Variables

Variable	Value	Variable	Value
A (m^2)	348	rp	1.25
dte (m)	0.0254	Ds (m)	0.940
dti (m)	0.0221	lay	2
L (m)	6.10	ltp (m)	0.03175
Nb	18	Ntt	715
Npt	4	ebc (m)	0.321

Table 14. Results for Case Study 1—Thermofluid Dynamic Variables

Variable	Value
ΔPs (Pa)	79138
ΔPt (Pa)	39435
hs (W/m^2K)	1104
ht (W/m^2K)	1795
U (W/m^2K)	632
vs (m/s)	0.74
vt (m/s)	1.74

Case study 2: Pressure drop manipulation

An important parameter in the design of a heat exchanger is the available pressure drop. This parameter represents a trade-off between pumping operational costs and heat exchanger capital costs. However, a more complete analysis of this issue must also consider fouling aspects.

Tables 15 and 16 show the result of the application of the design procedure in relation to Example 2, but allowing a 25% increase in the available pressure drop for the crude oil.

The analysis of the new solution indicates that the increase of the available pressure drop brought a reduction of the heat-transfer area from 412 to 396 m^2. This area reduction occurred because the higher available pressure drop allowed an increase of the tube-side heat-transfer coefficient, from 1646 to 2238 W/m^2K, and there was a total fouling suppression, that is, the heat exchanger associated to a higher pressure drop is inside the no fouling region.

This result indicates that the manipulation of the pressure drop can be a variable employed to mitigate fouling. Besides

Table 15. Results for Case Study 2—Design Variables

Variable	Value	Variable	Value
A (m^2)	396	rp	1.33
dte (m)	0.0254	Ds (m)	1.07
dti (m)	0.0221	lay	2
L (m)	6.10	ltp (m)	0.0338
Nb	18	Ntt	814
Npt	6	ebc (m)	0.321

Table 16. Results for Case Study 2—Hermofluid Dynamic Variables

Variable	Value
ΔPs (Pa)	34889
ΔPt (Pa)	98734
hs (W/m^2K)	808
ht (W/m^2K)	2238
U (W/m^2K)	560
vs (m/s)	0.52
vt (m/s)	2.30

Table 17. Results for Case Study 3—Design Variables

Variable	Value	Variable	Value
A (m^2)	585	rp	1.25
dte (m)	0.0254	Ds (m)	1.219
dti (m)	0.0221	lay	2
L (m)	6.10	ltp (m)	0.03175
Nb	19	Ntt	1203
Npt	6	ebc (m)	0.305

Table 18. Results for Case Study 3—Thermofluid Dynamic Variables

Variable	Value
ΔPs (Pa)	74001
ΔPt (Pa)	47833
hs (W/m^2K)	984
ht (W/m^2K)	1638
U (W/m^2K)	390
vs (m/s)	0.60
vt (m/s)	1.55

the possibility of capital costs reduction, the possibility to operate inside the no fouling region also has other advantages: elimination of costs associated to heat exchanger cleaning, elimination of environmental problems associated to the discard of the deposits, longer operational runs, and so forth.

Case study 3: Energy integration

The selection of the optimal set of heat exchanges in crude preheat trains is fundamental for the reduction of the fuel consumption in the fired heater located at the end of the train. This case study illustrates that fouling aspects may affect the problem of energy integration.

We use a design problem equivalent to Example 2, but all stream temperatures presented in Table 4 are increased by 20°C, thus representing a similar service that would be located at a different position along the crude preheat train. Because all temperatures were modified simultaneously, the temperature approach is the same and a conventional design procedure with fixed fouling resistances would yield the same result (dismissing possible modifications of physical properties).

However, the increase of the temperatures in the heat exchange task implies an increase of the surface temperature that intensify the fouling problem. This effect can be illustrated by Tables 17 and 18, where it is depicted the solution of the Example 2 with higher temperatures.

The original solution of Example 2 presents an area of 412 m^2 associated to a fouling resistance of $3.22 \cdot 10^{-5}$ m^2K/W (asymptotic fouling condition). The increase of the stream temperatures elevated the area to 585 m^2 and the fouling resistance to $7.04 \cdot 10^{-4}$ m^2K/W (maximum fouling condition).

The considerable difference in the heat exchanger area of similar thermal tasks, but associated to different temperature levels, is an indication of the importance of the inclusion of fouling modeling in the heat exchanger network synthesis. An example of the discussion of the relation between network synthesis and fouling modeling can be found in Wilson et al.[37]

Conclusions

This article presented a MILP formulation for the design of shell-and-tube heat exchangers including a fouling threshold model. This kind of a model can describe the behavior of fouling in crude oil streams subjected to higher temperatures in crude preheat trains of petroleum distillation units.

The insertion of a fouling model in the heat exchanger design optimization allowed the search to explore the relation between the thermofluid dynamic conditions of the solution candidates and the resultant fouling resistance. Therefore, the optimization can guide the search toward alternatives associated to a less severe deposit accumulation, which allows the utilization of smaller equipment. In certain problems, it is even possible to identify heat exchanger design solutions associated to a no fouling condition, where the heat exchanger can operate without deposit accumulation (however, in some other situations this condition is not feasible because is associated to excessively high velocities).

This analysis was illustrated using three examples, where in two examples, the proposed procedure identified cheaper design solutions when compared with a traditional approach which employs fixed fouling resistances. Associated to these examples, three case studies illustrated future opportunities of investigations relating the fouling modeling and heat exchanger design to broader problems involving crude selection, pressure drop optimization, and heat exchanger network synthesis.

Acknowledgments

André L. H. Costa thanks the National Council for Scientific and Technological Development (CNPq) for the research productivity fellowship (Process 311225/2016-0) and the financial support of the Prociência Program (UERJ). Conselho Nacional de Desenvolvimento Científico e Tecnológico, 311225/2016-0,;Universidade do Estado do Rio de Janeiro, Prociência Program.

Notation

A = area, m^2
$\widehat{Af}$ = fouling model parameter, m^2K/J
Ar = area between adjacent baffles, m^2
$\widehat{Bf}$ = fouling model parameter, m^2K/J
dte = outer tube diameter, m
dti = inner tube diameter, m
Deq = equivalent diameter, m
Ds = shell diameter, m
Ea = activation energy, J/mol
fs = Darcy friction factor on shell-side, dimensionless
ft = Darcy friction factor on tube-side, dimensionless
F = LMTD correction factor, dimensionless
FAR = free area ratio
FR = formation rate on fouling model, m^2K/J
FR_{min} = formation rate on fouling model for minimum surface temperature, m^2K/J
FR_{max} = formation rate on fouling model for clean surface, m^2K/J
$\widehat{g}$ = gravity acceleration, m/s^2
hs = convective heat transfer coefficient on shell-side, W/m^2K
ht = convective heat transfer coefficient on tube-side, W/m^2K
$\widehat{ks}$ = thermal conductivity of the shell-side stream, W/m·K
$\widehat{kt}$ = thermal conductivity of the tube-side stream, W/m·K
lay = layout of the heat exchanger
lbc = baffle spacing, m
ltp = tube pitch, m
L = tube length, m
$\widehat{ms}$ = mass flow rate on shell-side, kg/s
$\widehat{mt}$ = mass flow rate on tube-side, kg/s
Nb = number of baffles
Npt = number of tube passes
Ntp = number of tubes per pass
Ntt = total number of tubes
Nus = Nusselt number for shell-side
Nut = Nusselt number for tube-side

$\widehat{PDs}_{srow}$ = standard shell diameter, m
$\widehat{Pdte}_{srow}$ = standard outer tube diameter m
$\widehat{Pdti}_{srow}$ = standard inner tube diameter, m
$\widehat{PL}_{srow}$ = standard tube length, m
$\widehat{Play}_{srow}$ = tube layout
$\widehat{PNb}_{srow}$ = number of baffles
$\widehat{PNpt}_{srow}$ = number of tube passes
$\widehat{PNtt}_{srow}$ = total number of tubes
$\widehat{Prp}_{srow}$ = standard tube pitch ratio
$\widehat{Prs}$ = Prandtl number of the shell-side stream, dimensionless
$\widehat{Prt}$ = Prandtl number of the tube-side stream, dimensionless
$\widehat{Q}$ = heat load, W
R = ideal gas constant, J/mol K
rp = tube pitch ratio
Res = Reynolds number of the shell-side stream, dimensionless
Ret = Reynolds number of the tube-side stream, dimensionless
Rft = fouling resistance on tube-side, m^2K/W
$\widehat{Rf}^{MAX}$ = maximum fouling resistance on the tube-side, m^2K/W
Rf^{∞} = asymptotic fouling resistance on tube-side, m^2K/W
SR = suppression rate on fouling model, m^2K/J
$\widehat{Tc}^{av}$ = cold stream average temperature, K
$\widehat{Tci}$ = cold stream inlet temperature, K
$\widehat{Tco}$ = cold stream outlet temperature, K
$\widehat{Thi}$ = hot stream inlet temperature, K
$\widehat{Tho}$ = hot stream outlet temperature, K
Ts = surface temperature, K
Tw = wall temperature, K
U = overall heat transfer coefficient, W/m^2 K
vs = shell-side flow velocity, m/s
$\widehat{vsmax}$ = maximum shell-side flow velocity, m/s
$\widehat{vsmin}$ = minimum shell-side flow velocity, m/s
vt = tube-side flow velocity, m/s
$\widehat{vtmax}$ = maximum tube-side flow velocity, m/s
$\widehat{vtmin}$ = minimum tube-side low velocity, m/s
wRf = variable representing the fouling resistance, m^2K/W
$w1Rf^{\infty}$ = variable representing the asymptotic resistance, m^2K/W
$w2Rf^{\infty}$ = variable representing the asymptotic resistance, m^2K/W
$w3Rf^{\infty}$ = variable representing the asymptotic resistance, m^2K/W
$y1$ = binary variable to map the fouling resistance value
$y2$ = binary variable to map the fouling resistance value
$y3$ = binary variable to map the fouling resistance value
yd_{sd} = binary variable representing the tube diameter
yDs_{sDs} = binary variable representing the shell diameter
yL_{sL} = binary variable representing the tube length
$ylay_{slay}$ = binary variable representing the tube layout
yNb_{sNb} = binary variable representing the number of baffles
$yNpt_{sNpt}$ = binary variable representing the number of tube passes
yrp_{srp} = binary variable representing the tube pitch ratio
$yrow_{srow}$ = binary variable that represents simultaneously all discrete variables

Greek letters

α = fouling model parameter, m^2K/J
γ = fouling model parameter, m^2K/J
ΔPs = pressure drop on shell-side, Pa
$\Delta\widehat{Psdisp}$ = available pressure drop on shell-side, Pa
ΔPt = pressure drop on tube-side, Pa
$\Delta\widehat{Ptdisp}$ = available pressure drop on tube-side, Pa
$\widehat{\Delta T}^{av}$ = average temperature difference, K
$\widehat{\Delta Tlm}$ = logarithmic mean temperature difference, °C
$\widehat{\mu s}$ = viscosity of the shell-side stream, Pa·s
$\widehat{\mu t}$ = viscosity of the tube-side stream, Pa·s
$\widehat{\rho s}$ = density of the shell-side stream, kg/m^3
$\widehat{\rho t}$ = density of the tube-side stream, kg/m^3
$\widehat{\psi f}$ = threshold model parameter, K

Literature Cited

1. Kern DQ. *Process Hear Transfer*. New York: McGraw-Hill, 1950.
2. Serth RW. *Process Heat Transfer: Principles and Applications*. Amsterdam: Elsevier, 2007.
3. Cao E. *Heat Transfer in Process Engineering*. New York: McGraw-Hill, 2009.
4. Caputo AC, Pelagagge PM, Salini P. Heat exchanger optimized design compared with installed industrial solutions. *Appl Therm Eng*. 2015;87:371–389.
5. Jegede FO, Polley GT. Optimum heat exchanger design. *Chem Eng Res Des*. 1992;70(A2):133–141.
6. Reppich M, Kohoutek J. Optimal design of shell-and-tube heat exchangers. *Comput Chem Eng*. 1994;18:S295–S299.
7. Mizutani FT, Pessoa FLP, Queiroz EM, Hauan S, Grossmann IE. Mathematical programming model for heat-exchanger network synthesis including detailed heat-exchanger designs. *Ind Eng Chem Res*. 2003;42(17):4009–4018.
8. Ponce-Ortega JM, Serna-González M, Salcedo-Estrada LI, Jiménez-Gutiérrez AA. Minimum-investment design of multiple shell and tube heat exchangers using a MINLP formulation. *Chem Eng Res Des*. 2006;84(10):905–910.
9. Ravagnani MASS, Caballero JA. A MINLP model for rigorous design of shell and tube heat exchangers using the TEMA standards. *Chem Eng Res Des*. 2007;85(10):1423–1435.
10. Gonçalves CO, Costa ALH, Bagajewicz MJ. Shell and tube heat exchanger design using mixed-integer linear programming. *AIChE J*. 2017;63(6):1907–1922.
11. Gonçalves CO, Costa ALH, Bagajewicz MJ. Alternative mixed-integer linear programming formulations for shell and tube optimal design. *Ind Eng Chem Res*. 2017;56(20):5970–5979.
12. TEMA. *Standards of the Tubular Exchangers Manufactures Association*, 9th ed. New York: Tubular Exchanger Manufactures Association, 2007.
13. Shilling RL. Fouling and uncertainty margins in tubular heat exchanger design: an alternative. *Heat Transf Eng*. 2012;33(13):1094–1104.
14. Butterworth D. Design of shell-and-tube heat exchangers when the fouling depends on local temperature and velocity. *Appl Therm Eng*. 2002;22:789–801.
15. Polley GT, Wilson DI, Yeap BL, Pugh SJ. Use of crude oil threshold data in heat exchanger design. *Appl Therm Eng*. 2002;22(7):763–776.
16. Polley GT, Fuentes AM, Pugh SJ. Design of shell-and-tube heat exchangers to achieve a specified operating period in refinery preheat trains. *Heat Transf Eng*. 2011;32(3–4):314–319.
17. Nakao A, Valdman A, Costa ALH, Bagajewicz MJ, Queiroz EM. Incorporating fouling modeling into shell-and-tube heat exchanger design. *Ind Eng Chem Res*. 2017;56(15):4377–4385.
18. Lemos JC, Costa ALH, Bagajewicz MJ. Linear method for the design of shell and tube heat exchangers including fouling modeling. *Appl Therm Eng*. 2017;125:1345–1353.
19. Nesta J, Bennett CA. Fouling mitigation by design. In: *Proc Int Conf Heat Exchanger Fouling and Cleaning* – 2005. Vol RP2, Kloster Irsee, Germany, 2005:342–347.
20. Incropera FP, DeWitt DP, Bergman TL, Lavine AS. *Fundamentals of Heat and Mass Transfer*, 6th ed. New York: John Wiley & Sons, 2006.
21. Saunders EAD. *Heat Exchangers: Selection, Design and Construction*. New York: John Wiley & Sons, 1988.
22. Taborek J. Input data and recommended practices. In: Hewitt GF, editor. *Heat Exchanger Design Handbook*. New York: Begell House, 2008.
23. Taborek J. Performance evaluation of a geometry specified exchanger. In: Hewitt GF, editor. *Heat Exchanger Design Handbook*. New York: Begell House, 2008.
24. Bennett CA, Kistler RS, Nangia K, Al-Ghawas W, Al-Hajji N, Al-Jemaz A. Observation of an isokinetic temperature and compensation effect for high temperature crude oil fouling. In: *Proc Int Conf Heat Exchanger Fouling and Cleaning* – 2007. Vol RP5. Tomar, Portugal, 2007:32–42.
25. Ebert W, Panchal CB. Analysis of Exxon crude-oil slip stream coking data. In: Panchal CB, Bott TR, Somerscales EFC, Toyama S, editors. *Fouling Mitigation of Industrial Heat Exchange Equipment*. New York: Begell House, 1997.
26. Panchal CB, Kuru WC, Liao C, Ebert WA, Palen JW. Threshold conditions for crude oil fouling, In: Boot TR, Melo LF, Panchal CB, Somerscale EFC, editors. *Understanding Heat Exchanger Fouling and Mitigation*. New York: Begell House, 1999.
27. Polley GT, Wilson DI, Yeap BL, Pugh SJ. Evaluation of laboratory crude oil threshold fouling data for application to refinery pre-heat trains. *Appl Therm Eng*. 2002;22(7):777–788.
28. Nasr MRJ, Givi MM. Modeling of crude oil fouling in preheat exchangers of refinery distillation units. *Appl Therm Eng*. 2006;26(14–15):1572–1577.

29. Wilson DI, Polley GT, Pugh SJ. Ten years of Ebert, Panchal and the 'threshold fouling' concept. In: *Proc Int Conf Heat Exchanger Fouling and Cleaning* - 2005. Vol RP2. Kloster Irsee, Germany, 2005:25–36.
30. Wilson DI, Ishiyama EM, Polley GT. Twenty years of Ebert and Panchal - What next? *Heat Transf Eng*. 2015;38:669–680.
31. Wang Y, Yuan Z, Liang Y, Xie Y, Chen X, Li X. A review of experimental measurement and prediction models of crude oil fouling rate in crude refinery preheat trains. *Asia Pacific J Chem Eng*. 2015;10:607–625.
32. Ishiyama EM, Paterson WR, Wilson DI. Thermo-hydraulic channelling in parallel heat exchangers subject to fouling. *Chem Eng Sci*. 2008;63(13):3400–3410.
33. Floudas CA. *Nonlinear and Mixed-Integer Optimization: Fundamentals and Applications*, 1st ed. New York: Oxford University Press, 1995.
34. Polley GT, Wilson DI, Pugh SJ, Petitjean E. Extraction of crude oil fouling model parameters from plant exchanger monitoring. *Heat Transfer Eng*. 2007;28(3):185–192.
35. Asomaning S, Panchal CB, Liao CF. Correlating field and laboratory data for crude oil fouling. *Heat Transf Eng*. 2000;21:17–23.
36. Costa ALH, Tavares VBG, Borges JL, Queiroz EM, Pessoa FLP, Liporace FS, Oliveira SG. Parameter estimation of fouling models in crude preheat trains. *Heat Transf Eng*. 2013;34(8–9):683–691.
37. Wilson, DI, Polley, GT, Pugh, SJ. Mitigation of Crude Oil Preheat Train by Design. *Heat Transfer Eng*. 2002;23:24–37.

Manuscript received Aug. 23, 2017, and revision received Jan. 1, 2018.